Computational Methods for VCSEL Array Characterization and Control

Pawel Strzebonski[a], Harshil Dave[a], Katherine Lakomy[a], Nusrat Jahan[a], William North[a], and Kent Choquette[a]

[a]Electrical and Computer Engineering Department, University of Illinois, Urbana, Illinois, USA

ABSTRACT

Coherent optical coupling in VCSEL arrays introduces novel and desirable behaviors that can manifest themselves in many ways. We explore some of these behaviors using common characterization techniques but using large datasets, and show how we use computational data analysis methods to analyze datasets in an automated and scalable manner.

Keywords: Vertical cavity surface emitting lasers, Phased arrays, Machine learning, Semiconductor lasers, Spatial coherence, Algorithms, Data analysis, Coherence tuning

1. INTRODUCTION

Shown in Figure 1 are 2×1 photonic crystal VCSEL arrays. Such coherently-coupled VCSEL arrays exhibit numerous novel behaviors that may be attractive for various applications. However, in order to exploit coherent effects we must be able to design VCSEL arrays such that the elements of the array will optically couple. This requires developing characterization methods that identify the coherence properties of VCSEL arrays. In this work we will look at some of the behaviors of VCSEL arrays that arise from coherent coupling by exploring large experimental datasets and data analysis methods to identify and characterize coherence.

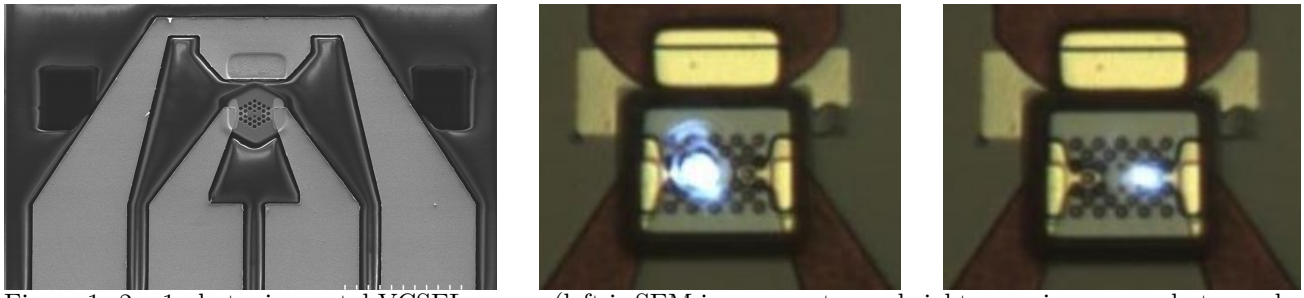

Figure 1: 2×1 photonic crystal VCSEL arrays (left is SEM image, center and right are microscope photographs with either the left or right cavity lasing).

2. THEORY

Arrays of two or more VCSELs may operate with various degrees of inter-element coherence. In the totally incoherent limit we can consider each element to be a independent device with its own localized optical mode. In the coherent limit we can consider the entire array to operate as a single optical cavity with an optical supermode that extends across all of the individual VCSELs. In between those two limits there are numerous situations where multiple modes may lase, with some optical modes spanning across multiple lasers (coherent array modes) and some possibly localized to individual lasers (incoherent element modes). The transition to and from coherent array mode operation can be observed in various laser parameters, including the laser spectra, far-field profile, output power, and differential resistance.[1]

Further author information: (Send correspondence to Pawel Strzebonski)
Pawel Strzebonski: E-mail: strzebo2@illinois.edu

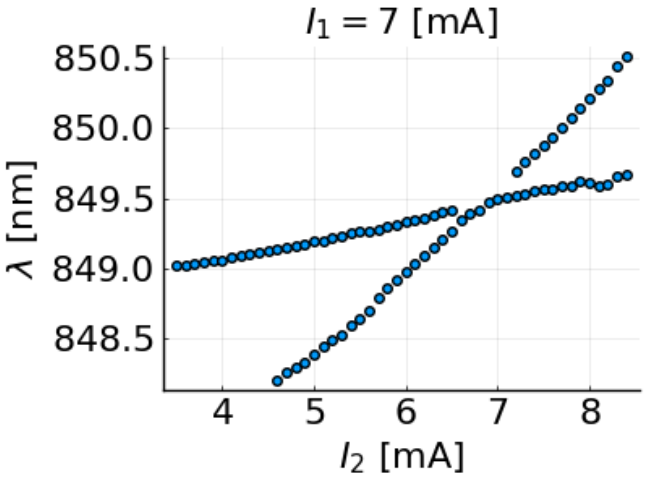

Figure 2: Spectral peaks as a function of driving current for a 2×1 array.

2.1 Spectral Characteristics

Let's consider a 2×1 VCSEL array at an incoherent operating point with both elements lasing. The optical spectrum will show multiple peaks corresponding to the lasing optical modes of the individual VCSELs. As the driving current to an element laser is tuned, the optical spectrum peaks for of laser element will shift. We can tune the driving currents of the individual VCSELs as to align the peaks of the element modes to the same wavelength. Coherent operation is observed when VCSELs are tuned as to align multiple spectral peaks into a peak.[2–5] As an example, consider Figure 2 which illustrates the peaks of the 2×1 VCSEL array optical spectrum as one of the driving currents is varied. We see that for most of the current range there are two distinct modal peaks, one for each of the array elements. However, as the current is tuned to about 7 [mA] the two peaks converge and merge into a single peak.

While the lasing of multiple VCSELs in an array with only a single spectral peak is associated with coherent operation, it is not necessarily a sufficient condition. For example only one element may be lasing, such as for currents less than 4.5 mA in Figure 2. Additionally, coherently coupled VCSEL arrays may display "locking" behavior whereby tuning the injection within a certain "locking range" of current values will cause the spectral peaks of several elements to align and join into a single peak.[6] In this case coherence is not evident simply a single discernible spectral peak in a single measurement, but rather in a series of spectral measurements showing a bias towards a single spectral peak as currents are tuned that deviates from the peak shifting during incoherent operation.

Of course, when there are more than two lasers or more than two modes in a single laser, there may be intermediate levels of coherence. For example, a VCSEL array comprised of a single mode element and a two mode element could have two coherently coupled regimes corresponding to the two combinations of the individual element's modes. In these cases we can still observe the same intersection and locking of spectral peaks, but the optical spectrum will show multiple peaks, some representing coherent array modes and some incoherent element modes.[4]

2.2 Far-Field Characteristics

The far-field of a laser is determined by the summation of the lasing modal far-fields. For example, a pair of un-coupled fundamental (Gaussian-like) modes in a 2×1 array will produce a far-field that is the superposition of the far-field for each of the two fundamental modes (a Gaussian-like far-field resulting from a superposition of two Guassian-like far-fields, as illustrated in Figure 3a). However, when the individual element modes are coherently coupled, this implies a two-lobed near-field with some phase difference between the two lobes (the

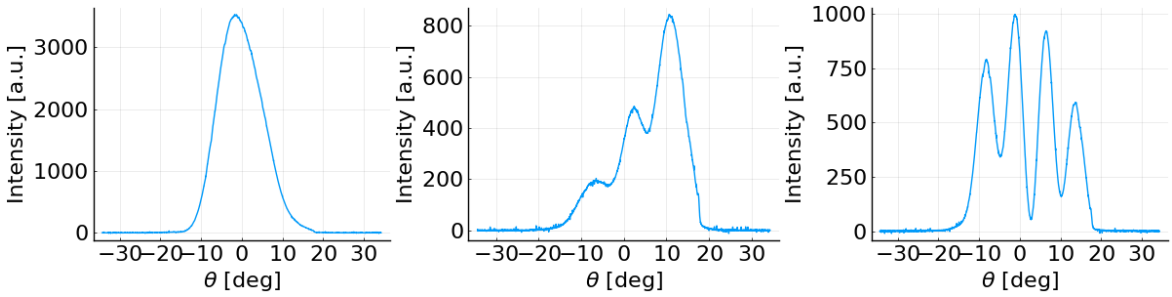

(a) $(I_1, I_2) = (7, 3)$ [mA] (b) $(I_1, I_2) = (5, 5)$ [mA] (c) $(I_1, I_2) = (5, 4)$ [mA]

Figure 3: 1D far-field images for the beam of a 2×1 VCSEL array at different driving currents.

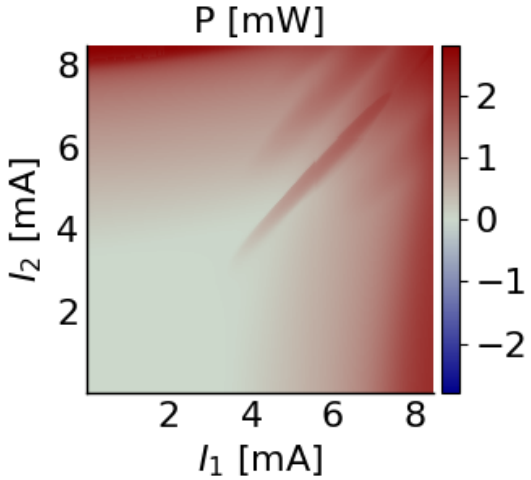

Figure 4: Optical power from 2×1 VCSEL arrays as a function of driving current.

exact phase relation between the lobes may vary depending on the array structure and injection), and the far-field is no-longer Gaussian-like but rather shows lobed structuring resulting from partial coherence, as shown in Figure 3b and Figure 3c. Such changes in the far-field profile have been observed not only in 2×1 arrays[1,4,5] but also in larger arrays, such as 2×2 arrays.[3]

This change from the Guassian-like far-field to a structured far-field as an array enters coherent operation is often quantified using the visibility parameter that relates the prominence of lobes in the far-field,[1,4,5] and coherence is often considered to occur when far-field visibility is relatively large (a value of 0 is considered fully incoherent, 1 fully coherent, and intermediate values relate intermediate levels of coherence). However, the far-field visibility parameter has some limitations. First, it assumes that the individual element modes are fundamental Gaussian-like modes. Second, when there are multiple lasing modes the far-fields for the individual modes superimpose in a manner that may obscure any underlying coherence. Third, it is uncertain to what extent the visibility parameter is appropriate for coupled arrays of three or more elements.

2.3 Optical Power Characteristics

Coherent coupling of VCSELs is associated with laser threshold lowering (relative to incoherent operation). This leads to coherent operation being associated with two phenomena. First is array mode lasing at driving currents that are below the threshold current for any element VCSEL.[1] Second is enhanced output power when operating coherently,[1,5] with the amount of increase power being related to the magnitude of the imaginary coupling coefficient.[7] This effect is well demonstrated in Figure 4

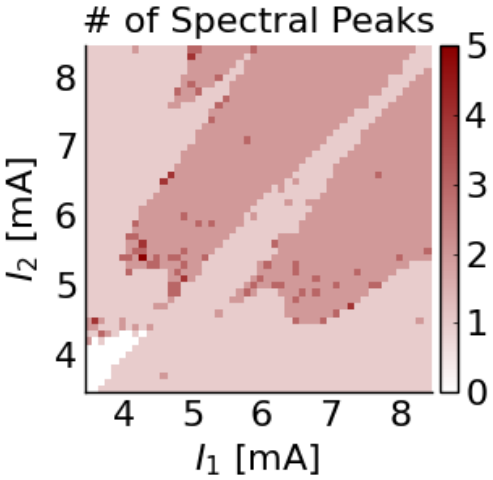

Figure 5: Spectral peak count as a function of driving current (Array from Figure 4).

Lasing below the threshold for the individual elements is a good indicator coherent operation. However, it is limited to identifying coherence in the sub-threshold current space. Perhaps for some applications operating in this relatively low power regime would be acceptable, the limited power and tuning range may not be acceptable for others.

The enhanced output power effect can be often observed in two-dimensional power versus driving current plots for 2×1 arrays as "ridges" of higher power (relative to the surrounding incoherent regions),[7] as in Figure 4. To what extent enhanced output power constitutes proof of coherence is not entirely certain as non-coherent effects may also induce features into the current–power curves.

2.4 Electrical Characteristics

It has been proposed that coherence in VCSEL arrays could be detected by purely electrical means by observing changes in the differential resistance.[8] It has been observed that there are peaks in the differential resistance when a VCSEL array is tuned in-to or out-of coherent operation.

3. COMPUTATIONAL METHODS

We describe and discuss some of the computational methods for analyzing various characteristics of VCSEL arrays for the identification of coherent operation. We focus on the simplest case of 2×1 arrays, although many of these methods can be generalized and applied to larger arrays.

3.1 Optical Spectrum Analysis

There are a couple potential methods of analyzing the modal and coherent behavior of VCSEL arrays using spectral data. First and simplest, we can consider how the number of modal peaks in the spectrum changes as the injection is varied. Second, we can try to model the modal peaks as a function of injection and use those models to identify where modes could couple.

3.2 Number of Spectral Modes

We scan the optical spectra as a function of driving current for the arrays whose power is plotted in Figure 4, identify the modal peaks in the spectra, and plot the number of identified peaks in Figure 5. While this metric appears to be somewhat noisy due to the errors in automated peak finding, it does reveal some trends that may indicate coherent operation. Namely, we can identify a region on the diagonal which has a single mode, surrounded by regions of 2 or more modes.

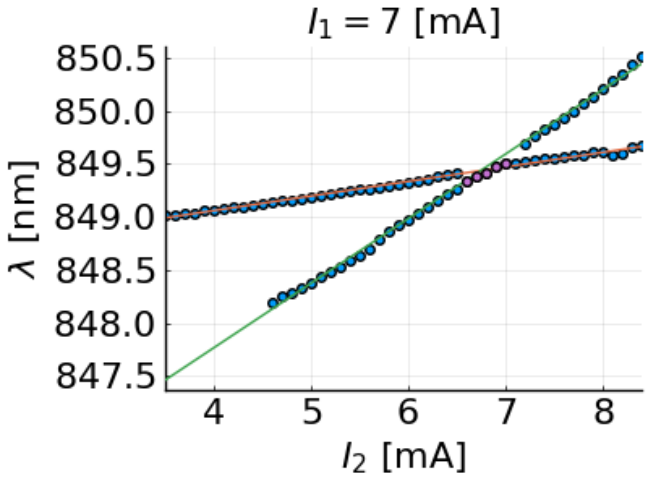

Figure 6: Line-fitting the spectral modes from Figure 2.

3.3 Modeling Spectral Modes

On the assumption that coupling between cavities will tend to occur when the element modes align in the spectrum, we could try to predict when the cavities will couple by analytically modeling the spectral modes and identifying where the intercept. However, this requires not only identifying the modal peaks in the spectra, but assigning them to specific element modes and deriving a current–wavelength relationship for those modes. If we assume that the spectral mode peaks vary linearly with respect to the driving current, this segmentation and regression problem reduces to identifying linear features in the set of measured current–wavelength points.

Many methods have been identified for identifying and modeling linear features in datasets. The Hough transform algorithm can be used to identify multiple linear features, not just lines in a 1D current scan but hyperplanes in higher dimensional spaces as well (enabling application of this analysis to larger arrays).[9] Furthermore, Hough transform methods may allow the spectral peak identification step to be bypassed. However, effectively extracting the current–wavelength relations for the modes from the Hough transform can be tricky. We have found that the RANSAC algorithm[10] can be effectively and intuitively applied to this problem by iteratively finding a linear fit for one of the modes among the spectral peak points and removing the points belonging to that mode before finding subsequent modes.

We use RANSAC to find and fit a pair of lines to the two spectral modes illustrated in Figure 2. We superimpose the fitted lines on the spectral peaks in Figure 6. Once the analytical models for the spectral peaks are obtained, one could solve directly for their intersections to predict where coherent coupling between those modes may be found (an advantage of this method being that one can take fewer spectral measurements that do not necessarily coincide with coherent operation, and then use additional targeted measurements to identify/verify coherence in the predicted coherent regimes). Alternatively, one can try to find spectral peaks for coherent array modes within a measured dataset by identifying measured points that are within a threshold distance to at-least two of the fitted spectral mode lines. For example, points within a small distance of both of the lines in Figure 6 are indicated in a different color. Naturally, these methods can be applied to scans of a greater number of driving currents and higher dimensionality (however the results are harder to visualize).

3.4 Far-Field Analysis

Much of the far-field analysis of VCSEL array coherence so far has focused on the visibility parameter, relating the difference between the maxima and minima in the far-field intensity. Visibility is defined as

$$\text{Visibility} = \frac{I_{\max} - I_{\min}}{I_{\max} + I_{\min}} \text{ or } \frac{\langle I_{\max}\rangle - \langle I_{\min}\rangle}{\langle_{\max}\rangle + \langle I_{\min}\rangle} \tag{1}$$

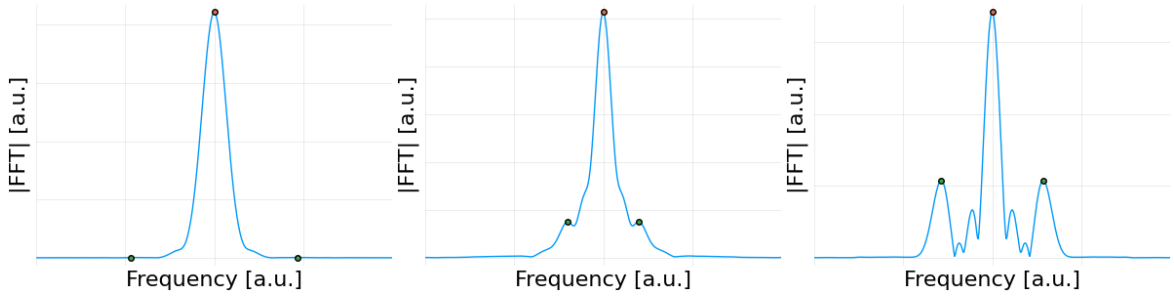

(a) $(I_1, I_2) = (7, 3)$ [mA] (b) $(I_1, I_2) = (5, 5)$ [mA] (c) $(I_1, I_2) = (5, 4)$ [mA]

Figure 7: Fourier transforms of the far-field images in Figure 3. The tallest, central peak (orange dot) represents the zero-frequency peak, while the surrounding peaks (green dots) represent the spatial frequency of the far-field interference fringes.

were $I_{\min}, I_{\max}$ are the values of the minima and maxima in the far-field intensity, respectively (the visibility may be calculated using the average values of the local minima and local maxima).[11,12] While this metric can be a good indication and measure of coherently coupled operation under certain conditions, it has various issues. First is the difficulty in calculation (especially automated calculation). The visibility calculation requires the proper identification of the maxima and minima related to the interference lobes in far-field intensity, which can be difficult in the case of noisy measurements. While this is possible to do, it can require fine-tuning the data pre-processing and peak-finding algorithm in order to consistently identify the correct maxima and minima. Second, the visibility as a measure of coherence is not defined for situations of more than two array elements, nor likely in cases of two elements with higher-order mode lasing.

We propose the use of Fourier methods to analyze far-fields. As coherence manifests itself as periodic interference fringes in the far-field, it also will manifest itself as non-zero frequency peaks in the Fourier transform of the far-field, as can be seen by comparing the far-fields in Figure 3 to their Fourier transforms in Figure 7. These non-zero frequency peaks can provide a few properties of the far-field and the coherence. The magnitude (relative to the zero frequency component, which is related to the total intensity fo the far-field) is indicative of the coherence, the frequency is indicative of the interference fringe spacing (which is related to the spacing of the near-field lobes), and the peak phase may be indicative of beam-steering (more-so for relative comparison as the tuning is changes than for absolute beam-steering angle determination). We find that this method is much more resilient to noise and algorithm parameters than the visibility method.

We collect a series of 1D far-field profile images for a 2×1 array for varied injection currents and we analyze the measurements. First, we estimate the optical power from each far-field profile as being proportional to the integral of the intensity profile, plotted in Figure 8a. We recognize a coherent ridge in the power measurement near the diagonal (but slightly off-set). Next, we calculate the far-field visibility an plot in Figure 8b. By comparing the optical power and far-field visibility plots we find that the visibility values tend to be high on the coherent ridge. However, we also find high visibility values off of the coherent ridge and a significant amount of noise in the visibility values which we attribute to error in visibility calculations due to difficulty in identifying the correct far-field minima and maxima.

Next, we calculate the Fourier transform of each far-field profile and analyze the non-zero frequency side-peaks in the Fourier transforms. We calculate and plot the ratio between the amplitude of the side-peak and the amplitude of the zero-frequency (DC) peak (representing the relative strength of the far-field interference fringes) in Figure 8c. Comparing to Figure 8a we find very good correspondence between the coherent power ridge and the high side-peak-to-DC-peak-ratio values. Furthermore, we find that this measure is much less noisy than the visibility values in Figure 8b. This Fourier analysis of far-field profiles appears to be simpler and more resilient than the previously used far-field visibility analysis for identifying coherent operation in VCSEL arrays.

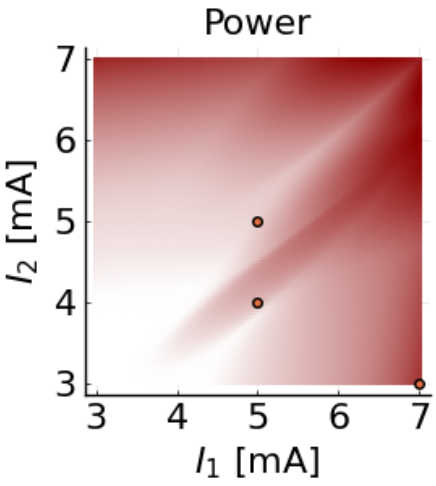

(a) Array Power

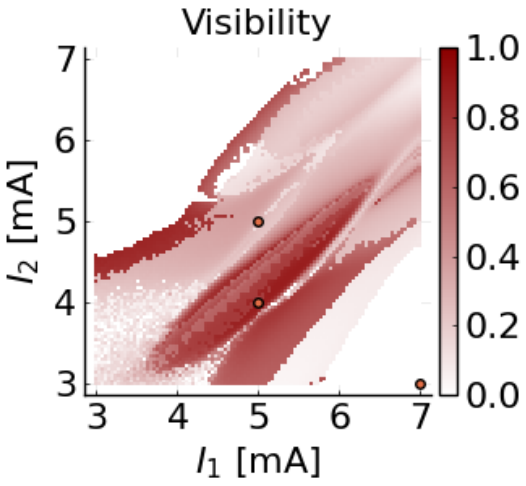

(b) Far-field visibility

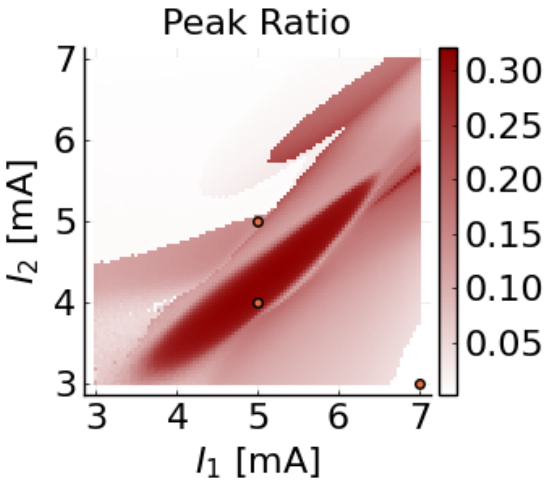

(c) Ratio of far-field FFT side-peak to DC peak

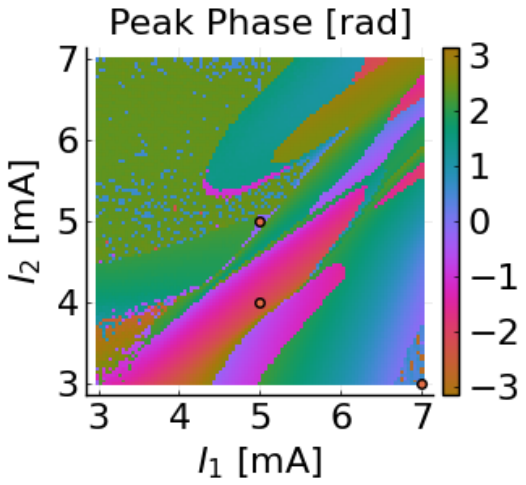

(d) Phase of far-field FFT side-peak

Figure 8: Mapping the power and far-field analysis of a 2×1 array as a function of driving current. Same array data as in Figure 3 and Figure 7, and locations of those far-field profiles are marked as dots.

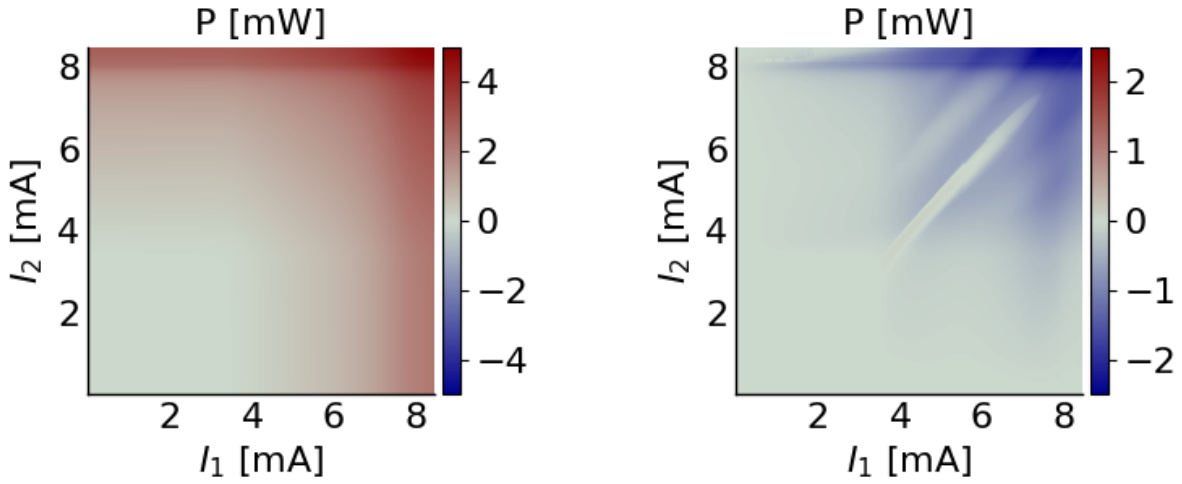

(a) Figure 4 data

(b) Figure 4 data

Figure 9: 9a represents "naive" incoherent array power predictions. 9b is the calculated "excess" power relative to predicted incoherent array power.

Furthermore, the phase of the Fourier transform side-peak can be used to analyze beam-steering of the coherent far-field. In Figure 8d we find that the side-peak phase in the coherent region tends to vary perpendicular to the ridge, indicating some degree of beam-steering as the driving current is tuned perpendicular to the diagonal.

3.5 Optical Power Analysis

We can consider two main approaches towards identifying coherence in optical power data. The first is value based, where we want to derive some sort of quantity from a single power measurement to classify whether that point is coherent or not. The second is feature based, were we classify whether or not a point is coherent based on multiple power measurement.

3.5.1 Optical Power Value

The coherence threshold lowering effect should lead to higher optical power during coherent operation versus incoherent operation. Therefore if one could predict the incoherent output power for any point and compare it to the measured power, the problem of determining coherence would be as simple as determining whether the measurement is significantly larger than the incoherent prediction. The difficulty lies in determining a reasonable prediction for the power.

The simplest method for predicting the incoherent output power is simply measuring the current-power curve for each individual element in the array and predicting the array power, $P_{\text{array,predicted}}(I_1, I_2, \dots)$, to be the summation of the power of the incoherent individual powers, $P_i(I_i)$:

$$P_{\text{array,predicted}}(I_1, I_2, \dots) = \sum_i P_i(I_i) \tag{2}$$

We calculate this predicted incoherent array power for the arrays whose power is illustrated in Figure 4 and plot it in Figure 9. The problem with this approach is that regardless of whether the array elements are coherently coupled or not, the current through one element will lead to a thermal threshold shift in the near-by elements (this thermal shifting of the power measurement can be observed in Figure 4), leading to $P_{\text{total,predicted}}(I_1, I_2, \dots)$ often being an overestimate of the incoherent array power. As such, the "excess" power due to coherence may be underestimated with this simple model, obscuring some regions of coherence. In Figure 9b there is hardly any excess power calculated due to the underestimation effect, although the coherent ridge is still obvious as having a greater (ie less negative) excess power than the surrounding areas.

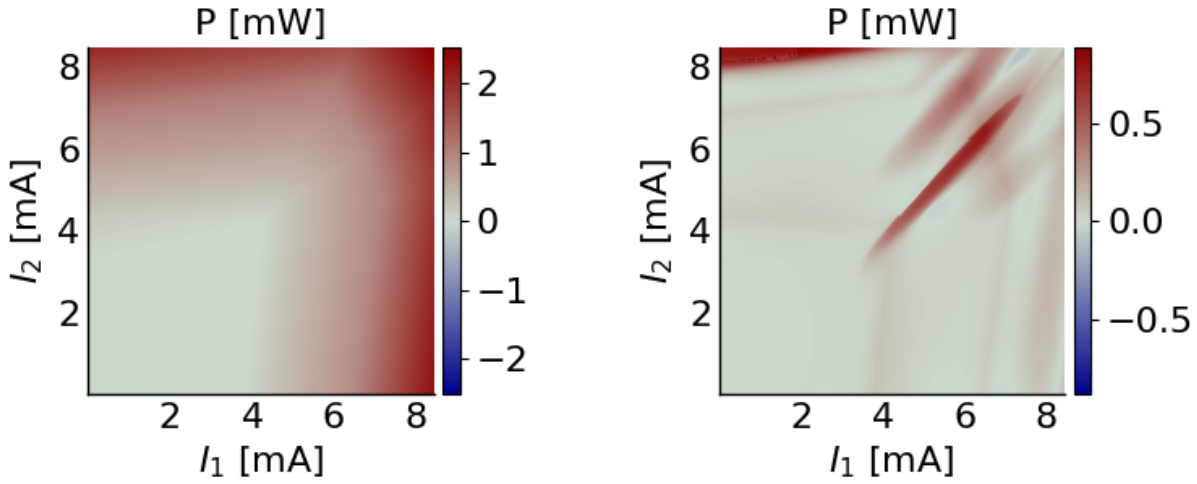

(a) (b)

Figure 10: 10a represents artificial neural network predictions incoherent array power. 10b is the calculated "excess" power relative to predicted incoherent array power (Figure 4 data).

A better way of estimating the uncoupled array power (one incorporating the shifting effects) from the measurements could enable reasonable power enhancement calculation, which would be useful not only for determining coherence but determining the imaginary coupling coefficient as well.[7] One can try to predict the uncoupled array power using machine learning methods using an artificial neural network that predicts the array power from a set of current values.

For a 2×1 array, we can use a small dense neural network to predict the power at each point given driving currents I_1, I_2 when trained on the measured current–power dataset (including both coherent and incoherent datapoints). With appropriate choice in layer width and network depth ($2 \to 3 \to 3 \to 1$ in our example) the network will tend to model the incoherent array power with all of the shifting effects but not the coherent power enhancement, allowing it to be used as an estimate of the incoherent power for power enhancement calculations. The loss function should not simply encourage fitting of the predicted power to the measured power, but also enforce some basic physical constraints, including that the array power should be positive and that it should be biased towards underestimation rather than overestimation of the total array power (as some underestimation would be expected due to coherent power enhancement effects). We create, train,[13] and use neural networks to get the predicted uncoupled array power and power enhancement illustrated in Figure 10. The estimated "excess" power in Figure 10 shows the coherent ridge on the diagonal very distinctly a positive value, consistent with the concept of coherent power enhancement, and does not show significant negative "excess" power as does Figure 9b.

However, the neural network approach can be a bit finicky to train and be a bit excessive to this particular problem. An alternative method is defining a set of analytical equations for the element power and total array power that can accommodate shifting effects, and fitting the coefficients to the measured dataset. We can incorporate the shifting effects to obtain effective shifting driving currents

$$I_{\mathrm{i,shifted}}(I_1, I_2, \dots) = \sum_j \alpha_{ij} I_j \tag{3}$$

where α_{ij} are empirical fitting coefficients that relate the shifting effects the injection into one cavity has on the other cavities. The individual element power can then be estimated as a polynomial in terms of the effective

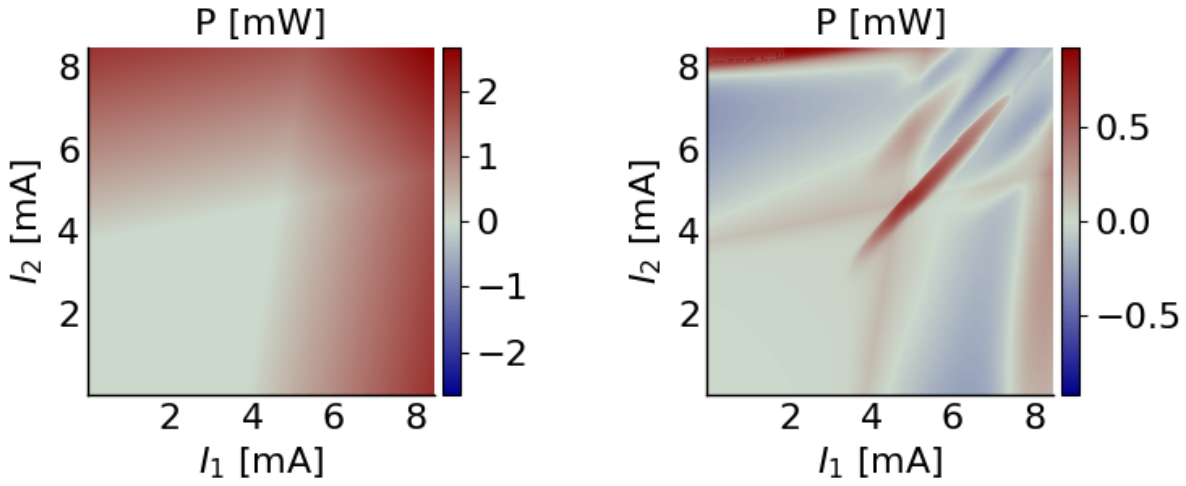

(a) (b)

Figure 11: 11a represents linear incoherent array power predictions. 11b is the calculated "excess" power relative to predicted incoherent array power (Figure 4 data).

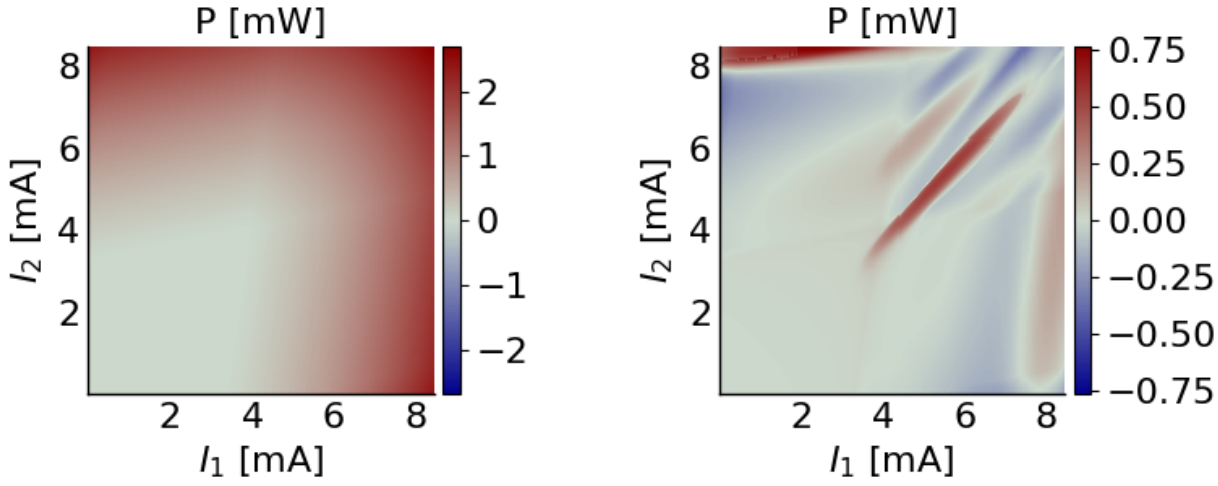

(a) (b)

Figure 12: 12a represents quadratic incoherent array power predictions. 12b is the calculated "excess" power relative to predicted incoherent array power (Figure 4 data).

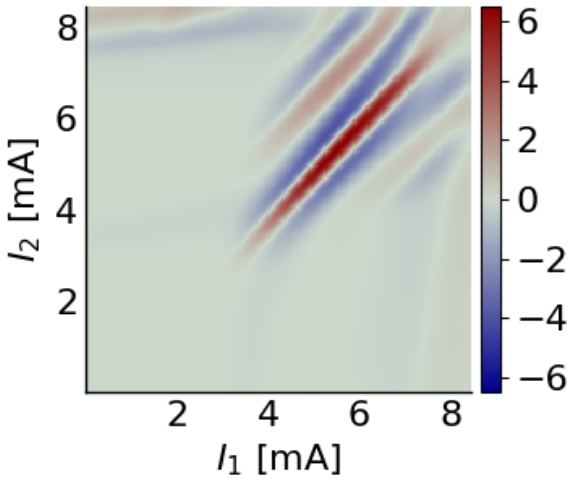

Figure 13: Ridge-feature cross-correlation for the power measurement data (Data from Figure 4).

element current

$$P_i(I_{\text{i,shifted}}) \approx \max\left(\sum_{j=0}^{N} \beta_{ij} {I_{\text{i,shifted}}}^{j}, 0\right) \tag{4}$$

where β_{ij} are empirical coefficients and N is the order of the polynomial. We then model the total array power as the sum of these estimated element powers. We apply this analytical approach to the power measurement in Figure 4, first using a linear fit in Figure 11 and then a quadratic fit in Figure 12. Naturally, the results can be rather varied, although the measurements in Figure 4 can be well modeled using these simple analytical models for the most part.

3.5.2 Optical Power Feature

We can also exploit the fact that coherent operation tends to form "bumps" or "ridges" in power scans. Given a power versus driving current scan, we can calculate the cross-correlation between the power measurement and an appropriate template for the ridge. Figure 4 is a great example of such a power ridge. We calculate the cross-correlation between the power measurements in Figure 4 and $(+1, +1)$ oriented ridge template and plot the results in Figure 13. The obvious ridge feature in 4 leads to large cross-correlation values in Figure 13.

3.6 Differential Resistance Analysis

The entering into and exiting from the coherently coupled region can be recognized in the change in voltage as the driving currents are changed. We calculate the differential resistance from the voltage measurements that accompanied the power measurements in Figure 4 and plot in Figure 14. Despite the noisiness of the measurement and calculated differential resistance (even after measurement preprocessing in the form of smoothing the voltage), we can see some local changes in the differential resistance that appear to correspond to the edges of the coherent power ridges. In Figure 14 it appears that the change in differential resistance can be in the form of an increase or a decrease in value, depending on which side of the coherent ridge the differential resistance is calculated.

While voltage based approaches seem attractive due to the potential simplicity of a purely electrical process, the differential aspect of this analysis makes it particularly sensitive to noise in measurement, as evident in Figure 14. Data preprocessing, such as the Gaussian smoothing performed on the voltage measurements, is limited in its ability to overcome noise, necessitating decreasing the noise in the measurement process.

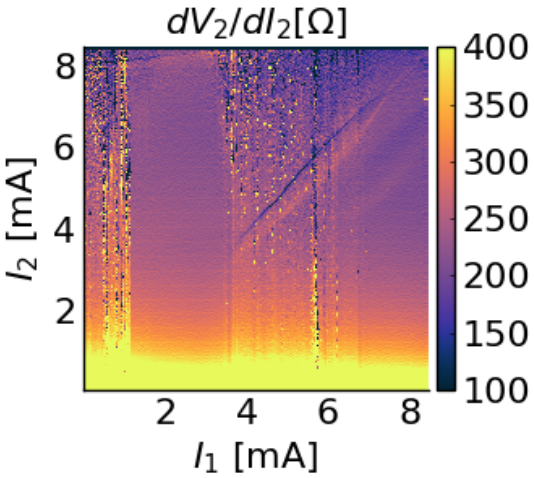

Figure 14: Calculated differential resistance as a function of driving current. Voltages had been smoothed in an attempt to overcome noise (Data from Figure 4).

4. METHODS COMPARED

Hardly any single measurement or analysis is by itself sufficient to prove coherent operation. Rather, multiple measurements/analyses or one measurement/analysis in combination with sufficient understanding of element and array behavior is needed to make a certain conclusion. We list the methods and their pros/cons in the following table.

Measurement	**Analysis**	**Pros**	**Cons**
Optical Spectrum	Peak Count	Can be strong indication of coherence Potential "single shot" analysis	Slow measurement Can fail due to spectral alignment of uncoupled modes
Optical Spectrum	Peak-Shift Modeling	Can be strong indication of coherence Potentially predictive of coherent operation conditions	Slow measurements Can fail due to spectral alignment of uncoupled modes Difficulty in accurately modeling multiple independent peaks
Far-Field Image	Visibility	Can be strong indication of coherence Potentially "single shot" analysis Relates strength of array coherence (for 2-element arrays operating in single fundamental mode)	Ill- or un-defined for larger arrays Ill- or un-defined when elements operate at higher order modes Tricky to properly calculate in automated fashion
Far-Field Image	Fourier Analysis	Relatively simple computational implementation Potentially "single shot" analysis Fairly rigorous against measurement noise	Not directly related to coherence May be bad metric if elements operate at higher order modes
Optical Power	Power Enhancement	Relatively simple measurement Related to strength of (imaginary) coupling coefficient	Requires accurate prediction of uncoupled power (impractical for certain array designs due to non-obvious power–current behavior) May be confused by other phenomena (switching between modes within a cavity)
Optical Power	Power Ridge	Relatively simple measurement Related to strength of (imaginary) coupling coefficient	Requires accurate prediction of uncoupled power (impractical for certain array designs due to non-obvious power–current behavior) May be confused by other phenomena (switching between modes within a cavity)
Voltage/Current	Differential Resistance	Fast and simple measurement	Noise sensitive

In the above table, "single shot" measurement and analysis refers to a method that can determine whether a device is operating coherently or not based on a single measurement point (without the need for multiple

measurements at various driving currents). Some analyses, such as peak-shift modeling, can be predictive of coherently coupled operation in the meaning that with sufficient measurements to obtain an accurate model, one may be able to infer potential driving currents that would lead to coherently coupled operation, even if none of the prior measurements were taken of coherently coupled operation.

5. CONCLUSION

Coherently coupled operation in VCSEL arrays can reveal itself in various measurements. We have shown and described how coherence can be observed in various measurements and discussed computational methods can assist in the automated analysis of these measurements.

REFERENCES

[1] Dave, H., Gao, Z., Fryslie, S. T. M., Thompson, B. J., and Choquette, K. D., "Static and dynamic properties of coherently-coupled photonic-crystal vertical-cavity surface-emitting laser arrays," *IEEE Journal of Selected Topics in Quantum Electronics* **25**, 1–8 (Nov. 2019).

[2] Fryslie, S. T. M., Johnson, M. T., and Choquette, K. D., "Coherence tuning in optically coupled phased vertical cavity laser arrays," *IEEE Journal of Quantum Electronics* **51**, 1–6 (Nov. 2015).

[3] Thompson, B. J., Gao, Z., Fryslie, S. T. M., Johnson, M. T., Siriani, D. F., and Choquette, K. D., "Coherence in multielement-phased vertical-cavity surface-emitting laser arrays using resonance tuning," *IEEE Photonics Journal* **9**, 1–8 (Oct. 2017).

[4] Dave, H., Liao, P., Fryslie, S. T. M., Gao, Z., Thompson, B. J., Willner, A. E., and Choquette, K. D., "Digital modulation of coherently-coupled 2×1 vertical-cavity surface-emitting laser arrays," *IEEE Photonics Technology Letters* **31**, 173–176 (Jan. 2019).

[5] Gao, Z., Thompson, B. J., Dave, H., Fryslie, S. T. M., and Choquette, K. D., "Non-hermiticity and exceptional points in coherently coupled vertical cavity laser diode arrays," *Applied Physics Letters* **114**, 061103 (Feb. 2019).

[6] Fryslie, S. T. M., Gao, Z., Dave, H., Thompson, B. J., Lakomy, K., Lin, S., Decker, P. J., McElfresh, D. K., Schutt-Aine, J. E., and Choquette, K. D., "Modulation of coherently coupled phased photonic crystal vertical cavity laser arrays," *IEEE Journal of Selected Topics in Quantum Electronics* **23**, 1–9 (Nov. 2017).

[7] Dave, H., Gao, Z., and Choquette, K., "Complex coupling coefficient in laterally coupled microcavity laser diode arrays," *Applied Physics Letters* **117**, 041106 (July 2020).

[8] Dave, H., Hwang, J., Gao, Z., and Choquette, K. D., "Electrical detection of coherent coupling in vertical cavity phased laser arrays," in [*2019 IEEE Photonics Conference (IPC)*], IEEE (Sept. 2019).

[9] Ballard, D., "Generalizing the hough transform to detect arbitrary shapes," *Pattern Recognition* **13**, 111–122 (Jan. 1981).

[10] Fischler, M. A. and Bolles, R. C., "Random sample consensus," *Communications of the ACM* **24**, 381–395 (June 1981).

[11] Gao, Z., *Non-Hermitian aspects of coherently coupled vertical cavity laser arrays*, PhD thesis, University of Illinois at Urbana-Champaign (08 2018).

[12] Dave, H., *Enhanced digital modulation of coherently coupled vertical cavity laser arrays: theory and application*, PhD thesis, University of Illinois at Urbana-Champaign (05 2019).

[13] Innes, M., "Flux: Elegant machine learning with julia," *Journal of Open Source Software* **3**, 602 (May 2018).